Signature of Short-Range van der Waals Forces Observed in Poisson Spot Diffraction with Indium Atoms

Nicolas Gack,[1] Christian Reitz,[1] Joshua Leo Hemmerich,[2] Max Könne,[2] Robert Bennett,[2,3] Johannes Fiedler,[2,4] Herbert Gleiter,[1] Stefan Yoshi Buhmann,[2] Horst Hahn,[1] and Thomas Reisinger[1]

[1]*Institute of Nanotechnology, Karlsruhe Institute of Technology, Hermann-von-Helmholtz-Platz 1, D-76344 Eggenstein-Leopoldshafen, Germany*

[2]*Physikalisches Institut, Albert-Ludwigs-Universität Freiburg, Hermann-Herder-Str. 3, D-79104 Freiburg i. Br., Germany*

[3]*School of Physics & Astronomy, University of Glasgow, Glasgow G12 8QQ, United Kingdom*

[4]*Centre for Materials Science and Nanotechnology, Department of Physics, University of Oslo, P.O. Box 1048 Blindern, NO-0316 Oslo, Norway*

(Received 13 December 2019; revised 29 April 2020; accepted 6 July 2020; published 27 July 2020)

The phase of de Broglie matter waves is a sensitive probe for small forces. In particular, the attractive van der Waals force experienced by polarizable atoms in the close vicinity of neutral surfaces is of importance in nanoscale systems. It results in a phase shift that can be observed in matter-wave diffraction experiments. Here, we observe Poisson spot diffraction of indium atoms at submillimeter distances behind spherical submicron silicon dioxide particles to probe the dispersion forces between atoms and the particle surfaces. We compare the measured relative intensity of Poisson's spot to theoretical results derived from first principles in an earlier communication and find a clear signature of the atom-surface interaction.

DOI: 10.1103/PhysRevLett.125.050401

Dispersion forces are a subtle phenomenon on a macroscopic scale but are of major importance in nanosystems. One of the most sensitive techniques used for the study of the associated interaction potential on a fundamental level is matter-wave diffraction. The minute attraction of atoms or molecules to neutral solid surfaces gives rise to a phase shift in their de Broglie wave functions, which can be detected in the resulting diffraction patterns. The dominant interaction is often called van der Waals (vdW) interaction. It was already predicted by Lennard-Jones [1] in 1932 to be of the form $V = -C_3/z^3$ for a plane surface. This approximation is expected to be valid away from a repulsive region at close approach and a region farther off where retardation effects can no longer be neglected. Depending on the community, the name Casimir-Polder interaction is used to refer to the retarded interaction or simply to stress that it is a force between an atom and a surface. The Poisson spot (PS) matter-wave diffraction [2–4] reported here is particularly sensitive to vdW forces in the nonretarded intermediate range. The attractive forces result in an enhanced intensity of the on-axis interference spot (PS) in the shadow cast by a sphere. The enhancement is due to an effective widening of the Fresnel zones close to the sphere, which is more pronounced at smaller sphere-detector distances b.

Traditionally, the vdW potential played a key role in thermal-energy atom-surface scattering [5]. In later developments diffraction and interferometry with artificial free-standing gratings have been demonstrated [6–9], yielding precise values for the C_3 constants for various rare gas atoms, alkali elements, as well as deuterium molecules at silicon nitride surfaces. Matter-wave diffraction is also used to probe interaction potentials between atoms as well as molecules [10,11] and provided proof for the existence of the fragile helium dimer [12,13]. Even in the limit of atomically thin grating structures, the vdW potential has been shown to substantially affect matter-wave diffraction [14]. On the one hand, the vdW interaction can be seen as a hindrance for this reason. This is especially the case in fundamental diffraction experiments that seek for deviations from the wave-particle duality [15,16]. The problem can be partially overcome by the use of gratings composed of standing light waves [17,18]. On the other hand, vdW forces are expected to be a major parameter affecting biomaterials, which can also be studied using matter-wave diffraction [19].

In this Letter we show that the phase shift due to the vdW potential can be observed with PS matter-wave diffraction. This is in contrast to previous PS experiments [3,4] where the vdW potential was not observed. The difference is that here we used a more polarizable effusive beam species, namely indium atoms. Compared to the previously used deuterium molecules, the static polarizability of indium is about an order of magnitude larger. Furthermore, we reduced the detection distance b (see Fig. 1) at which the spot is observed to the submillimeter range, in contrast to most atom diffraction experiments where the detection distance is normally of the order of 1 m [20]. This increases the sensitivity to the vdW potential, since it reduces the width of the Fresnel zone adjacent to the spherical obstacle. As diffraction objects spherical submicron particles

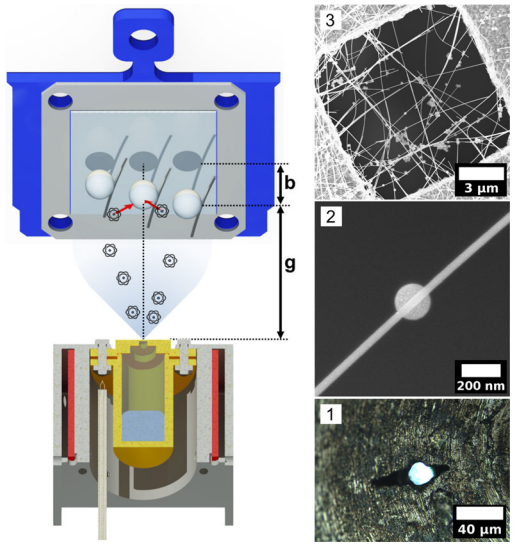

FIG. 1. Schematic of the Poisson spot experiment. Indium is evaporated in an effusive oven source with the indium atoms emanating from an orifice in the crucible lid [(1) optical micrograph]. They accumulate a phase shift due to the attractive vdW potential when passing the spherical submicron particles [attached to silver nanowires on copper grids: (2), (3) scanning electron micrographs], which are mounted at various detection distances b from a silicon wafer surface. There the Poisson spot diffraction images are recorded by condensation. Note the deposited indium in inset (2).

composed of silicon dioxide were chosen. The particles can be synthesized [21] with near-perfect spherical shapes, which is crucial for the observation of the PS. The perfect geometry facilitates modeling of the vdW potential and diffraction with full detail, which we have performed for the present experiment. We demonstrate that the observed diffraction intensities match well with theory.

The matter-wave PS diffraction experiment was performed in a two-chamber ultrahigh-vacuum setup (see Fig. 1) with a base pressure of 5×10^{-8} mbar. Observation of the PS requires a source of waves with sufficient spatial coherence, which was realized here using an effusive thermal oven source for indium (99.99% purity) with a laser-drilled nozzle of conical shape [(86 ± 5)–(19 ± 2) μm in diameter, 0.5 mm long]. Using two ceramic heating elements (Momentive) and a type-C thermocouple, the source temperature was kept at $T_s = (1746\pm10)$ K. At this temperature, indium has a vapor pressure of approximately 1850 Pa [22]. With a resulting mean free path of about 20 μm [23] (assuming a hard-sphere model and vdW radius 193 pm [24]), a few collisions between indium atoms while traversing the nozzle are to be expected. However, any effects from a gas-dynamic expansion can be safely neglected. The chamber pressure rose to as much as 1×10^{-6} mbar during evaporation.

The atomic beam is characterized by a broad speed distribution [25] of the form $(2/\alpha^4)v^3\exp(-v^2/\alpha^2)$ with $\alpha=\sqrt{2k_BT_s/m}$ and a most probable beam speed of $v_p=\sqrt{3/2}\alpha$. With T_s from above and the atomic mass of the indium atoms $m = 114.8$ u [26], we have obtained $v_p = 616$ m/s and therefore the central de Broglie wavelength of the beam can be calculated to be $\lambda_p = 5.64\times10^{-12}$ m.

Besides high spatial coherence, the surface corrugation of the spherical diffraction objects is critical in PS diffraction. Its height must be significantly less than that of the adjacent Fresnel zone w_{FZ} [27], which ranges from 3 to 9 nm in the present experiment. This is difficult to achieve with conventional lithography, which motivated the following bottom-up approach. We used solution-grown spherical silica particles [21] as diffraction objects and attached them to silver nanowires (Blue Nano, Inc.) on a standard copper transmission electron microscopy grid (Plano, 1500 mesh). Details of the preparation procedure are given in the Supplemental Material (SM) [28]. The grids were locked into position at distances b from the silicon wafer piece using laser-cut stainless steel sheets (0.05 mm thickness) as frames and spacers.

To detect the indium atoms we deposited them onto a silicon wafer piece (Si-Mat, Si100, n doped, 10×10 mm^2) at a distance from the source orifice of $g+b=(613\pm3)$ mm and subsequently imaged the indium thin film with scanning electron microscopy (SEM). To reduce formation of islands during film growth, we first deposited subnanometer layers of chrome followed by copper (see SM [28]). The total time for the indium deposition was 23 h and 34 min. The SEM images were recorded with the in-lens detector of a Zeiss (Leo) 1530 electron microscope (5 kV beam energy, 30 μm aperture, 8.4 mm working distance, scan speed 9). We assume a linear relation between the secondary electron count and the thickness of the indium film, while possible nonlinear contributions due to the film's morphology or the proximity effect are neglected. Here we report relative intensities $I_{\mathrm{rel}} = (I - I_{\mathrm{bg}})/(I_0 - I_{\mathrm{bg}})$, with measured secondary electron count rate per pixel I that includes a background intensity I_{bg} and intensity of the unobstructed wave front in the detection plane I_0.

The diffraction images, with the PS at the center, recorded for different b on the silicon wafer piece are shown in the SEM images in Fig. 2 together with diffraction images computed by solving the Fresnel-Kirchhoff diffraction integral with (FK + vdW) and without (FK) the vdW phase shift. The SEM image pixels were averaged using a Gaussian blur (3×3) matrix filter.

In order to determine the lateral intensity data shown in Fig. 3, we used a MATLAB script that selects two adjacent equally sized pie sections (see Fig. 2) centered at the particle shadow from the image, such that the influence of the supporting nanowire's shadow is excluded. Each pie section was then divided into 70 radial intervals of width 3.6 nm and the average pixel intensity calculated for each. In order to get the best estimate for the on-axis intensity, all

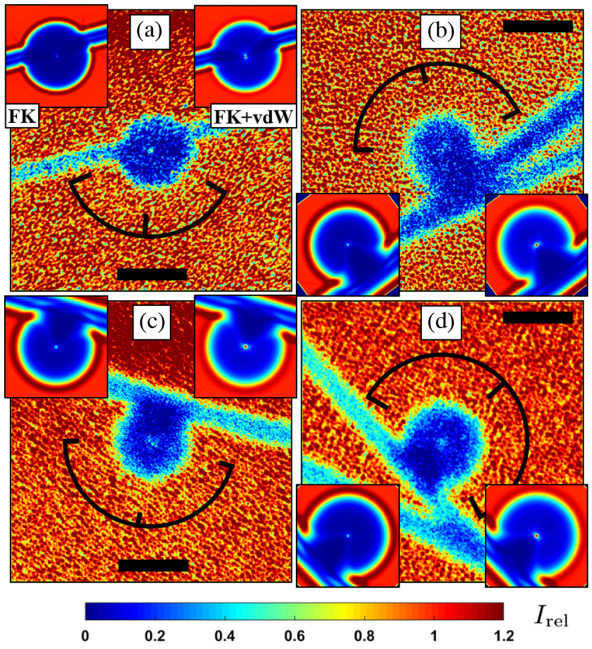

FIG. 2. Scanning electron micrographs of the indium film deposited on the silicon wafer piece. The shadows cast by the silver nanowires and spherical silicon dioxide particles are visible. Distinct Poisson spots are visible at the centers of the spherical-particle shadows. The right and left insets show the corresponding results of the Fresnel-Kirchhoff diffraction simulation with (FK + vdW) and without (FK) the phase shift due to vdW forces, respectively. The transmission electron microscopy grid supporting the wires or particles are mounted at detection distances $b = 0.1$ mm (a), 0.25 mm (b), and 0.3 mm (c),(d). The diameters of the spheres are (a) 176 nm, (b) 179 nm, (c) 181 nm, (d) 199 nm. The two adjacent pie sections indicated in each image correspond to the integration areas used for the lateral intensity data shown in Fig. 3. The scale bar length is 200 nm.

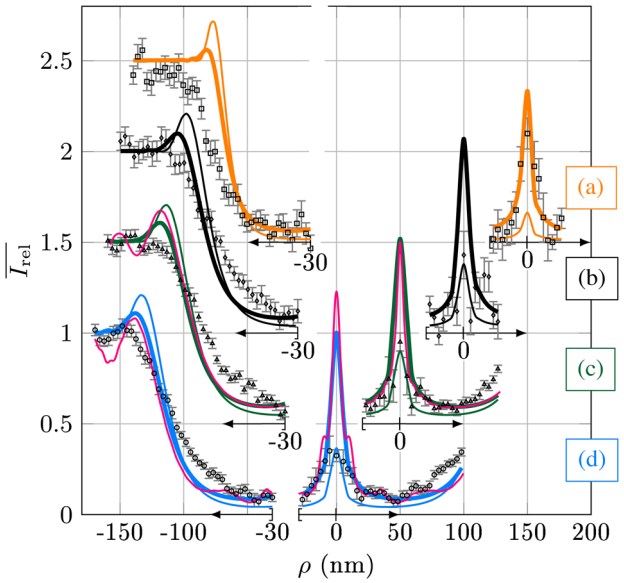

FIG. 3. Radial relative intensity extracted from the filtered SEM images in Figs. 2(a)–2(d) (data points; for error bars see text) and images from diffraction models by averaging of the same radial intervals. Shadow shoulders and central peak of (a)–(c) are shifted in steps of (10, 0.5) and (50,0.5) for clarity, respectively. The thick and thin lines are the result of the diffraction model taking and not taking into account a vdW potential, respectively, using the expected distribution of de Broglie wavelengths. The models include the blocking effect of the supporting wires [30 nm width in (a); in (b)–(d) the wire was assumed to be tangential to the sphere], but neglect surface corrugation. The thin pink lines in (c) and (d) show the FK + vdW model for a monochromatic beam at the central wavelength using the above averaging intervals and parallel to the wire's axis without averaging, respectively.

pixels near the optical axis where assigned to the innermost interval, lifting the angular restriction for that interval only. The error bars show an estimate of the uncertainty, and correspond to ± 1 standard deviation of the intensities divided by the square root of $1/9$ (estimated autocorrelation) times the number of pixels in each interval. As a consequence, the uncertainties at the inner intervals with the smallest pixel number (4–10) are comparatively large. The undisturbed intensity of the wave front could be well estimated from the images. However, we could not directly measure the background intensity for the images and have therefore set it by fitting the lowest intensity in the shadows to the simulated diffraction patterns (FK + vdW model in Figs. 2 and 3, and for each model separately in Fig. 4).

The rather sharp Poisson spot expected from the models is washed out mainly due to surface diffusion, but also due to vibration, thermal drifts, and the limited resolution of the SEM images in the experiment. All of these accumulate to the reduced slope of the observed shadow edges. For an accurate comparison between theory and data, we have thus averaged the on-axis peak intensity in extended circular regions that include the entire observed peak in Fig. 4.

In Fig. 2–4 we compare the diffraction data to two different numerical solutions of the Fresnel-Kirchhoff diffraction integral for each shadow cast by particle and wire. One simulation (FK + vdW model) includes a phase shift due to the vdW potential from the interaction with the sphere (the vdW interaction with the wire is disregarded in both models) while the other (FK model) does not. Details of the models for the PS intensity have been published before [27,29,30]. The potential was calculated for all sphere sizes and atomic distances in Ref. [29], where it was shown that for the present experiment it is sufficient to use what is there termed the large sphere, nonretarded approximation resulting in a phase shift given by

$$\Delta\varphi_{\mathrm{vdW}}(a) \approx \frac{C_3}{2\hbar v}\frac{3\pi\sqrt{R}}{2\sqrt{2}a^{5/2}}, \quad \text{for } a \ll R, \tag{1}$$

where R is the sphere radius, a is the distance from the sphere's surface, and $C_3 \approx 9.77 \times 10^{-50}$ Jm^3 as calculated

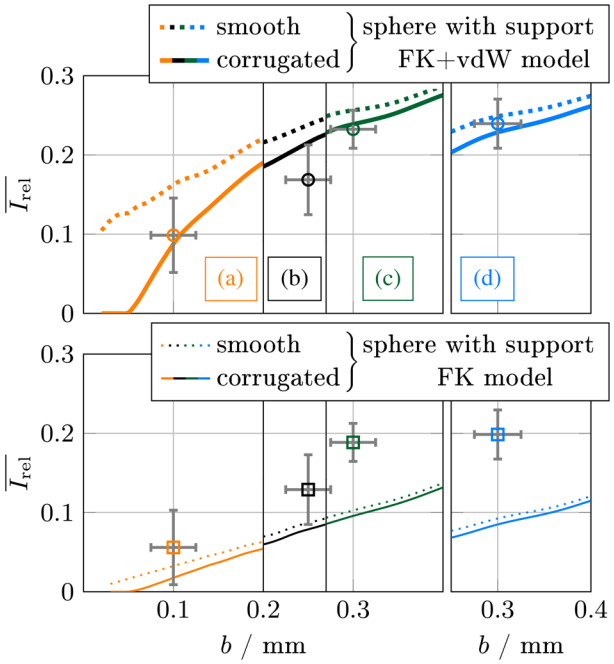

FIG. 4. Averaged relative intensity within 20 nm of shadow center for the models with (top panel, dotted line) and without (bottom panel, dotted line) taking the vdW interaction into account. The diffraction images of the on-axis spot were computed for b in steps of 0.01 mm at the central wavelength. The small (less than 10%) effect of the wavelength spread was corrected for by extrapolating the relative correction known exactly at the experiment's b values within each b range. For the data points we averaged over the same regions but using the SEM images in Fig. 2 (see SM [28]). The relative intensities are adapted for the differing shadow minima in the two models. The estimated reduced intensities due to surface corrugation of 1.5 nm, as determined from atomic force microscopy (see SM), are indicated using continuous lines. Within the indicated b ranges the specific sphere and wire parameters associated with the data points have been used. The data points clearly correspond better to the model taking vdW interactions into account.

from the indium polarizibility and silicon dioxide permittivity [29]. The sphere radii were determined from the average diameters of the shadows. Here we have additionally accounted for the broad speed (wavelength) distribution of the atomic beam. To this end, the diffraction patterns for atomic speeds v ranging from 16 to 1231 m/s (31 to 1201 m/s)—about twice the full width at half maximum—at intervals of 15 m/s (30 m/s) were evaluated for the FK (FK + vdW) model and then the average taken, weighted according to the speed distribution. In Fig. 3(c) the result of a monochromatic beam at λ_p and of a beam with the speed distribution noted above are compared. As expected I_{rel} of the PS are nearly identical and oscillations at the shadow's edge are nearly washed out. In Fig. 3(d) we additionally show that some of the fringes in the shadow match well with the monochromatic FK + vdW model without interval averaging. This would suggest that the beam's speed distribution was more narrow. However, since the features stem from diffraction with the supporting wire (see SM [28]) its vdW interaction with the atoms would have to be included to reach a more detailed conclusion.

The simulation data shown in Figs. 2 and 3 assume smooth spheres (without surface corrugation). Since modeling of a peak-to-peak surface corrugation σ_{corr} of the spheres directly in the diffraction integral is computationally expensive, we estimate its effect in Fig. 4 by using the factor $\cos^2[(\pi/2)(\sigma_{\mathrm{corr}}/w_{\mathrm{FZ}})]$ for the resulting attenuation of I_{rel} on axis [27] in both models as a function of b (See SM [28]).

The comparison of averaged on-axis intensities shown in Fig. 4 reveals a clear signature of the vdW phase shifts. In particular, the data points in Figs. 4(c) and 4(d) are not compatible with the model disregarding vdW interactions. The film deposited on the spheres (about 5 nm) likely increased surface corrugation during the experiment, further reducing the expected intensities. However, the metallic layer increases the strength of the vdW potential counteracting the latter effect from corrugation [29]. In addition, the lack of increased intensity observed in the experiment at the shadow edges, as can be noted in Figs. 2 and 3, is more compatible with the FK + vdW model.

We cannot exclude the existence of charges on the surface of the silica spheres. However, we expect that the phase shift from charges would be orders of magnitude stronger than the relatively small vdW phase shift, and therefore simply wash out the PS. This is a possible explanation for the reduced visibility or even lack of it in some shadows. Other possible reasons include motion of the particle during indium deposition and surface defects on the sphere's surface. In total, we recorded about 50 images of particle shadows. The PS was clearly visible in only 10 of them.

Studying the effect of various types of surface functionalization of the silica spheres on the vdW potential is an interesting prospect. Such studies could provide important input for the improvement of matter-wave diffractive optics via vdW phase shifts [31–33].

Finally, an exciting aspect of the experiment is the question of whether the quantum nature of the silica spheres themselves affects the diffraction experiment. The diffraction of an indium atom results in a transfer of momentum to the shadow-casting sphere, and it is thus required that this momentum be within the momentum uncertainty of the sphere [14]. If this was not the case, the recoil of the sphere could be measured in principle, and reveal which-way information about the path taken by the indium atom, causing decoherence. While in far-field single-slit diffraction experiments the recoil momentum will be of the order $\Delta p \approx h/a$, where h is Planck's constant and a the slit width [34], in the present experiment atoms appearing at the shadow's center must have received a momentum kick of $\Delta p \approx h/(2\lambda b/d)$. An uncertainty of the

position of the sphere of about 6 nm or less, considering the $b = 0.1$ mm diffraction image, would ensure that the transferred momentum is within the momentum uncertainty of the sphere. This is certainly the case here. However, in the future cavity-based ground-state cooling of levitated nanospheres [35–38] may sufficiently reduce momentum uncertainty, enabling the measurement of the sphere's recoil for each passing atom.

In the present experiment we have observed Poisson's diffraction spot with indium atoms in the shadow of dielectric spheres at submillimeter detection distances. We show that the relative intensity of Poisson's spot is increased due to the phase-shifting vdW potential between sphere and atom. The diffraction simulation corresponds well to the experimental data. Further reduction of the effects that laterally diffuse Poisson's spot would increase sensitivity to the vdW interaction and thus open the possibility of measuring vdW phase shifts for many materials relevant in nanosystems.

We thank Markus Arndt for fruitful discussions. Support from the Deutsche Forschungsgemeinschaft is acknowledged by S. Y. B., J. F., and R. B. (Grants No. BU 1803/3-1 and No. BU 1803/6-1) as well as H. H. (Grant No. DFG 1344/24-1). J. F. acknowledges support from the Research Council of Norway (Project No. 250346). T. R. acknowledges support by the Ministry of Science, Research and Art of Baden-Württemberg via a Research Seed Capital (RISC) grant, as well as the Helmholtz Association.

[1] J. E. Lennard-Jones, Trans. Faraday Soc. **28**, 333 (1932).
[2] S. Nowak, N. Stuhler, T. Pfau, and J. Mlynek, Phys. Rev. Lett. **81**, 5792 (1998).
[3] T. Reisinger, A. A. Patel, H. Reingruber, K. Fladischer, W. E. Ernst, G. Bracco, H. I. Smith, and B. Holst, Phys. Rev. A **79**, 053823 (2009).
[4] T. Reisinger, G. Bracco, and B. Holst, New J. Phys. **13**, 065016 (2011).
[5] D. Farias and K.-H. Rieder, Rep. Prog. Phys. **61**, 1575 (1998).
[6] R. E. Grisenti, W. Schöllkopf, J. P. Toennies, G. C. Hegerfeldt, and T. Köhler, Phys. Rev. Lett. **83**, 1755 (1999).
[7] D. W. Keith, C. R. Ekstrom, Q. A. Turchette, and D. E. Pritchard, Phys. Rev. Lett. **66**, 2693 (1991).
[8] J. D. Perreault and A. D. Cronin, Phys. Rev. Lett. **95**, 133201 (2005).
[9] J. D. Perreault, A. D. Cronin, and T. A. Savas, Phys. Rev. A **71**, 053612 (2005).
[10] T. Reisinger, M. M. Greve, S. D. Eder, G. Bracco, and B. Holst, Phys. Rev. A **86**, 043804 (2012).
[11] T. Reisinger, G. Bracco, S. Rehbein, G. Schmahl, W. E. Ernst, and B. Holst, J. Phys. Chem. A **111**, 12620 (2007).
[12] W. Schöllkopf and J. P. Toennies, Science **266**, 1345 (1994).
[13] R. E. Grisenti, W. Schöllkopf, J. P. Toennies, G. C. Hegerfeldt, T. Köhler, and M. Stoll, Phys. Rev. Lett. **85**, 2284 (2000).
[14] C. Brand, M. Sclafani, C. Knobloch, Y. Lilach, T. Juffmann, J. Kotakoski, C. Mangler, A. Winter, A. Turchanin, J. Meyer, O. Cheshnovsky, and M. Arndt, Nat. Nanotechnol. **10**, 845 (2015).
[15] M. Arndt and K. Hornberger, Nat. Phys. **10**, 271 (2014).
[16] S. Nimmrichter and K. Hornberger, Phys. Rev. Lett. **110**, 160403 (2013).
[17] S. Gerlich, L. Hackermueller, K. Hornberger, A. Stibor, H. Ulbricht, M. Gring, F. Goldfarb, T. Savas, M. Mueri, M. Mayor, and M. Arndt, Nat. Phys. **3**, 711 (2007).
[18] Y. Y. Fein, P. Geyer, P. Zwick, F. Kiałka, S. Pedalino, M. Mayor, S. Gerlich, and M. Arndt, Nat. Phys. **15**, 1242 (2019).
[19] M. Sclafani, T. Juffmann, C. Knobloch, and M. Arndt, New J. Phys. **15**, 083004 (2013).
[20] T. Juffmann, H. Ulbricht, and M. Arndt, Rep. Prog. Phys. **76**, 086402 (2013).
[21] W. Stöber, A. Fink, and E. Bohn, J. Colloid Interface Sci. **26**, 62 (1968).
[22] F. Geiger, C. A. Busse, and R. I. Loehrke, Int. J. Thermophys. **8**, 425 (1987).
[23] H. Pauly, *Atom, Molecule and Cluster Beams I* (Springer, New York, 2000).
[24] S. Alvarez, Dalton Trans. **42**, 8617 (2013).
[25] *Atomic, Molecular, and Optical Physics: Atoms and Molecules*, edited by F. B. Dunning and R. G. Hulet, Experimental Methods in the Physical Sciences Vol. 29B (Academic Press, San Diego, 1996).
[26] J. Meija, T. B. Coplen, M. Berglund, W. A. Brand, P. De Bièvre, M. Gröning, N. E. Holden, J. Irrgeher, R. D. Loss, T. Walczyk, and T. Prohaska, Pure Appl. Chem. **88**, 265 (2016).
[27] T. Reisinger, P. M. Leufke, H. Gleiter, and H. Hahn, New J. Phys. **19**, 033022 (2017).
[28] See Supplemental Material at http://link.aps.org/supplemental/10.1103/PhysRevLett.125.050401 for additional information on experimental methods and simulations.
[29] J. L. Hemmerich, R. Bennett, T. Reisinger, S. Nimmrichter, J. Fiedler, H. Hahn, H. Gleiter, and S. Y. Buhmann, Phys. Rev. A **94**, 023621 (2016).
[30] M. Könne, R. Bennett, T. Reisinger, and S. Y. Buhmann, Phys. Rev. A **96**, 013626 (2017).
[31] T. Reisinger, S. Eder, M. M. Greve, H. I. Smith, and B. Holst, Microelectron. Eng. **87**, 1011 (2010).
[32] M. Koch, S. Rehbein, G. Schmahl, T. Reisinger, G. Bracco, W. E. Ernst, and B. Holst, J. Microsc. **229**, 1 (2008).
[33] M. Barr, A. Fahy, J. Martens, A. P. Jardine, D. J. Ward, J. Ellis, W. Allison, and P. C. Dastoor, Nat. Commun. **7**, 10189 (2016).
[34] O. Nairz, M. Arndt, and A. Zeilinger, Phys. Rev. A **65**, 032109 (2002).
[35] D. Windey, C. Gonzalez-Ballestero, P. Maurer, L. Novotny, O. Romero-Isart, and R. Reimann, Phys. Rev. Lett. **122**, 123601 (2019).
[36] U. Delić, M. Reisenbauer, D. Grass, N. Kiesel, V. Vuletić, and M. Aspelmeyer, Phys. Rev. Lett. **122**, 123602 (2019).
[37] M. Rashid, M. Toroš, A. Setter, and H. Ulbricht, Phys. Rev. Lett. **121**, 253601 (2018).
[38] U. Delić, M. Reisenbauer, K. Dare, D. Grass, V. Vuletić, N. Kiesel, and M. Aspelmeyer, Science **367**, 892 (2020).